

Analytical Study of Quasi-One-Dimensional Flat Band Networks and Slow Light Analogue

A. NANDY

Department of Physics, Kulti College, Kulti, Paschim Bardhaman, West Bengal-713 343, India

(Received January 12, 2019; revised version February 18, 2019; in final form February 25, 2019)

Exact method of analytical solution of flat, non-dispersive eigenstates in a class of quasi-one-dimensional structures is reported within the tight-binding framework. The states are localized over certain sublattice sites. One such finite size cluster of atomic sites is decoupled from the rest of the system by the special “non-permissible” vertex having zero amplitude. This immediately leads to the *self-trapping* of the incoming excitation. We work out an analytical scheme to discern the localizing character of the diffraction free dispersionless modes using real space renormalization group technique. Supportive numerical calculations of spectral profile and transport are demonstrated to substantiate the essence of compact localized states. Possible experimental scope regarding the photonic analogue of the tight-binding electronic case is also discussed elaborately. This eventually unfolds the concepts of *slow light* and the related re-entrant mode switching from the study of optical dispersion.

DOI: [10.12693/APhysPolA.136.164](https://doi.org/10.12693/APhysPolA.136.164)

PACS/topics: delocalization, quasiperiodicity, thermoelectricity, renormalization

1. Introduction

There are several translationally invariant lattices in the tight-binding description that ensure the existence of one (or more) entirely dispersionless flat band(s) in the spectrum and hence are called flat band (FB) networks. Lattice systems containing flat bands have been of great interest over the recent few years.

In general, the localization phenomenon incidentally happens due to the presence of disorder. This is the celebrated case of the Anderson localization [1]. After completion of half century of it, the subject is still alive in many aspects of condensed matter physics. Although there are some special low-dimensional networks present where excitation can be localized even in absence of any disorder and thus the corresponding single particle eigenstate forms a completely momentum independent flat band in the whole Brillouin zone. Due to the phase cancellation in the presence of local spatial symmetries wave excitation does not diffuse beyond the periphery of a finite sublattice sites in cases of several low-dimensional networks. This brings the essence of *self-localization*. This is in complete contrast to the canonical case of the Anderson localization where exponential localization is caused by disordered environment. Comparatively, *compact localized states* (CLS) typically occur in overall periodic systems. Such CLSs are used for the formation of tunable, local symmetry-induced bound states in an energy continuum. The key fact is the destructive kind of quantum interference resulting from the local topological symmetry present in the underlying geometry. This also implies the well-known flat band localization where the quenched kinetic energy of the particle leads to complete

immobility of the electron. The specific topology of the system has a strong influence on the overall spectrum and in most of the cases, it induces remarkable spectral features introducing dispersionless flat bands in several low-dimensional networks.

The journey of flat band network started almost thirty years ago from Sutherland’s prediction [2] of flat band and the corresponding state is “strictly localized” in the dice lattice (which relates to previous research on quasi-periodic lattices and the Penrose tilings). This section of study had an initial interest in the field of strongly correlated systems because of having an open platform in the context of ferromagnetism [3–8]. The nearly FB states having non-zero Chern number supports an interesting physics regarding the fractional quantum hall effect [9–12]. Starting from all these things this area has extended its impact on several branches of condensed matter physics. Extensive studies have been done related to gapped FB states or gapless chiral modes in graphenes [13], optical lattices of ultracold atoms [14], wave guide arrays [15], and in microcavities having exciton-polaritons [16].

Several tight binding lattices are studied in the context of this flat band localization. Kagomé, Lieb, diamond, AB_2 stub, and sawtooth lattices are some vivid examples of the flat band lattices, and some general methods [17–22] are proposed to design more lattice structures with flat bands. Many theoretical works related to the flat band lattices have been done in the context of ferromagnetism [23], superconductivity [24], and the Wigner crystals [25–27]. Theoretical understanding is based on simplified models or approximations and comparison with experiment is crucial.

Recent interest in this area has arisen due to experimental realization of flat band systems [28, 29] in the Lieb photonic lattices and tight-binding photonic bands in metallophotonic waveguide networks [30]. Such flat

e-mail: atanunandy1989@gmail.com

photonic bands are intimately connected to the path-breaking idea of engineering slow light [31] with low group velocity which opens up the possibility of “spatial compression of light energy”. The most intriguing property of the flat band is the localization of the wave function at certain sublattice sites. The single particle wave function is finite within a cluster of atomic sites but becomes zero at some connecting nodes, making it impossible to escape from those finite size clusters of atomic sites. The quenched kinetic energy suppresses the quantum transport of the wave train and the group velocity vanishes. This immobility corresponding to such *self-localized* modes eventually contribute to non-dispersive part of the energy-wave vector relation. The singular behaviour arising out of the immobility is expected to produce anomalous behavior in the physical properties, transport, and optical responses. Another interesting fact about FB is that the dispersion curve is essentially flat in curvature for that specific energy. This implies that the single particle energy state is independent of the momentum of the particle. This brings a concept of divergent effective mass tensor i.e., the particle behaves like a super-heavy one and the immediate immobility severely affects the transport of quantum mechanical wave packet that results in some unconventional phenomena such as inverse Anderson transition [32]. Moreover, these FB systems can be classified into two separate categories according to the response to the external perturbation, particularly uniform magnetic flux, or any kind of disorder effect. This first category [33, 34] do not display flat bands for finite magnetic flux. In contrast, the Lieb class of lattices exhibits robustness of the FB, i.e., the FB remains unperturbed in respect of application of external magnetic flux.

In a flat band, diffraction is totally suppressed due to destructive interference, in a way analogous to geometric frustration, giving rise to eigenmodes that are compactly localized in space. Contrary to the canonical case of the Anderson localization, for those compact localized states, wave excitations strictly vanish outside a finite size sublattice of a system and this is entirely caused by destructive interference in the presence of local spatial symmetries. The immediate application of CLS lies in the information transmission [35–37] and directly stems from their compactness. Because of extremely low mobility of the wave packet CLS does not spread out spatially during evolution. CLSs are suitable candidates for the transmission of signal along photonic wave guide arrays avoiding “crosstalk” between waveguides [29]. Moreover, CLSs essentially enable the appearance of isolated bound states within a scattering continuum [38, 39].

The principal motivation behind this article is to look into possibility of demonstration of a general analytical scheme within the tight-binding formalism to discern the flat non-dispersive states for quasi-one-dimensional structures. The states are essentially localized over clusters of atomic sites and one such trapping cluster is effectively isolated from the rest of the network. This is partially

by the destructive quantum interference and partially by the physical boundary formed by the sites with vanishing amplitude. We have discussed a decoupling technique to analyze those self-localized pinned states where there is no overlap between the wave functions of the neighboring nodes corresponding to such energy. This confirms the localized nature of the dispersionless modes.

The tight-binding analogy with the electronic case and the corresponding photonic scenario helps us to propose a monomode waveguide network made of the same geometry. We present here a simple analytical method to detect the sharply localized photonic eigenmodes that are pinned on certain atoms or atomic clusters in a periodic array of diamonds. The non-dispersive character of such states is explicitly worked out. The other point of interest in the present work is to analyze the distribution of the amplitudes of such flat-band states in real space.

We find interesting results. We have been able to work out a method to extract the flat band modes for a set of quasi-one dimensional structures. The non-diffusive nature of such non-dispersive states is also confirmed. The presence of both dispersionless and dispersive states leads to an interesting situation of mode crossover.

Before we end this section, it is worth mentioning that single-mode wave guides have recently been fabricated and used in a quasiperiodic optical setup [40] to unravel topological states in quasicrystals. Localization transition in one-dimensional quasiperiodic lattices has also been investigated experimentally in recent times [41]. Also quite recently, the computational design of flat band models [42, 43] has enriched this section of study. The present proposal, to our mind, can thus be tested with an appropriately designed wave guide network.

2. Description of model and analysis: rhombic lattice

2.1. Spectral information by RSRG method

We start our discussion with the prototype example of AB_2 rhombic lattice (Fig. 1). The electron’s hopping is restricted between the nearest neighboring sites only. According to the number of nearest neighbours we distinguish between two types of sites, viz., one with coordination number three and colored in blue (named as B sites) and the other, black circles, having a coordination number four (A sites). Spinless non-interacting electrons are described by the tight-binding Hamiltonian in the Wannier basis,

$$H = \sum_m \epsilon_m c_m^\dagger c_m + \sum_{\langle mn \rangle} t_{mn} [c_m^\dagger c_n + \text{h.c.}] . \quad (1)$$

In the above expression ϵ_m is the on-site energy term at the respective quantum dot location that gives the potential contribution and t_{mn} is the nearest neighbor hopping parameter (or *overlap integral*) carrying the kinetic signature. Depending on the coordination number ϵ_m can assume values equal to ϵ_3 or ϵ_4 according to the local connection. It is needless to say that without any

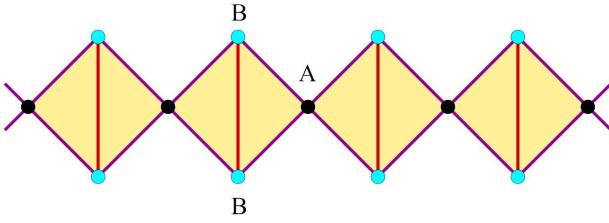


Fig. 1. A portion of an infinitely long quasi-one dimensional AB_2 rhombic lattice.

loss of generality we just assign the numerical values of ϵ_3 and ϵ_4 both equal to zero throughout the analytical calculation since we are interested to see the effect of topology of the lattice. The vertical connection (shown as solid line) between the top and the down vertices is taken as λ . The difference equation which is an alternative discretized form of the Schrödinger equation can be written as follows:

$$(E - \epsilon_m)\psi_m = \sum_n t_{mn}\psi_n. \quad (2)$$

2.2. Analytical construction of compact localized state

We will follow the real space renormalization group technique to discern the non-dispersive *compact localized* state. By virtue of the above expression one can easily decimate out the central vertices in terms of the amplitudes of the surviving nodes to map *effectively* it into a two-arm ladder network Fig. 2a comprising identical atomic nodes with ‘effective’ on-site potential $\tilde{\epsilon} = \epsilon_3 + \frac{2t^2}{(E - \epsilon_4)}$. The overlap integrals will also be renormalized and function of energy. The hopping along each arm of the ladder now becomes $\tau = t^2/(E - \epsilon_4)$ and the inter-arm vertical connection becomes $\gamma = \lambda + 2t^2/(E - \epsilon_4)$. This decimation procedure following RSRG technique creates a second neighbour connection i.e., diagonal hopping integral $\chi = t^2/(E - \epsilon_4)$.

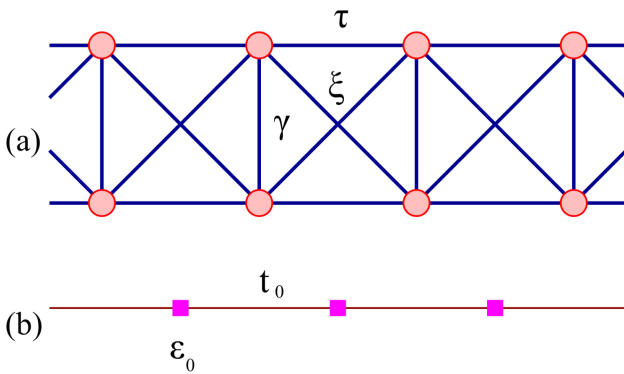


Fig. 2. (a) The *effective* two-arm ladder with the *renormalized* parameters (all the sites have the same on-site potentials $\tilde{\epsilon}$) and (b) The *renormalized* periodic linear chain of identical atomic sites. This scheme helps to compute the dispersion relation.

With all these *renormalized* parameters we can now rewrite the difference equation for this effective two-legged ladder geometry. The equation can be written as,

$$(E - \tilde{\epsilon})\psi_{n,A} = \tau(\psi_{n+1,A} + \psi_{n-1,A}) + \gamma\psi_{n,B} + \xi(\psi_{n+1,B} + \psi_{n-1,B})$$

$$(E - \tilde{\epsilon})\psi_{n,B} = \tau(\psi_{n+1,B} + \psi_{n-1,B}) + \gamma\psi_{n,A} + \xi(\psi_{n+1,A} + \psi_{n-1,A}) \quad (3)$$

The above equation for the coupled system can be easily cast in a composite matrix form using the potential and hopping matrices in the form,

$$\left[\begin{pmatrix} E & 0 \\ 0 & E \end{pmatrix} - \begin{pmatrix} \tilde{\epsilon} & \gamma \\ \gamma & \tilde{\epsilon} \end{pmatrix} \right] \begin{pmatrix} \psi_{n,A} \\ \psi_{n,B} \end{pmatrix} = \begin{pmatrix} \tau & \xi \\ \xi & \tau \end{pmatrix} \begin{pmatrix} \psi_{n+1,A} \\ \psi_{n+1,B} \end{pmatrix} + \begin{pmatrix} \tau & \xi \\ \xi & \tau \end{pmatrix} \begin{pmatrix} \psi_{n-1,A} \\ \psi_{n-1,B} \end{pmatrix}. \quad (4)$$

Now, one important point to be mentioned here is that the forms of the potential matrix (comprising the on-site energy and vertical connection) and the hopping matrix (connecting τ and χ) are such that they will commute, and hence can be simultaneously diagonalized by a similarity transform. So taking the advantage of this commutation, we can make a uniform change of basis defined by $\phi_n = M^{-1}\psi_n$ and the coupled difference equation for ladder can now be easily decoupled into a set of two independent difference equations for the two arms. The matrix M makes both the potential and hopping matrices diagonal. The decoupled set of equations are now obviously free from any coupling term (that makes the inter-arm connection) and read in terms of the original lattice parameters as

$$\left[E - \left(\epsilon_3 + \lambda + \frac{4t^2}{E - \epsilon_4} \right) \right] \phi_{n,1} = \frac{2t^2}{E - \epsilon_4} (\phi_{n+1,1} + \phi_{n-1,1}),$$

$$[E - (\epsilon_3 - \lambda)] \phi_{n,2} = 0. \quad (5)$$

The first one immediately represents a perfectly ordered chain of identical atomic sites with energy dependent renormalized on-site potential $\epsilon_3 + \lambda + \frac{4t^2}{(E - \epsilon_4)}$ and the effective overlap parameter $t = \frac{4t^2}{(E - \epsilon_4)}$. The second equation represents the difference equation (in the new basis) of an *isolated atom* with effective on-site energy. The corresponding wave function does not have any overlap with the wave function envelope of the neighboring nodes, i.e., completely isolated from the rest of the system. The eigenstate is a CLS, in the spirit of Bodyfelt et al. [44], which is localized partially by the destructive kind of quantum interference and partially by the physical boundary formed by the sites with zero amplitudes. The topology of the system concerned is the key reason for the perfect geometric phase cancellation.

This leads to an eigenfunction with amplitudes *pinned* at the top and down vertices and the eigenvalue corresponding to this pinned localized state is $E = \epsilon_3 - \lambda$. The amplitude distribution is shown pictorially in Fig. 3. The incoming wave train having this particular energy will be trapped in the local clusters (vertices with coordination number equal to three) and will show no evolution dynamics. This macroscopically degenerate state gives a momentum independent contribution in the $E - k$ dispersion curve and is therefore called an FB state [45], a locus of zero mobility points in the momentum space near the Fermi level.

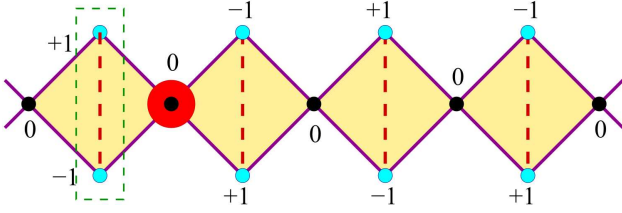


Fig. 3. Amplitude distribution for the *flat band* state at $E = \epsilon_3 - \lambda$. The green encircled area shows the characteristic *trapping cell* and the red circle shows the zone that is not permissible for electron because of the nodes having zero amplitude.

2.3. Density of states

Before looking for the non-dispersive nature of the compact localized state supported by this quasi-one-dimensional structure, it is generally advisable to have the overall idea of the allowed eigenspectrum for such a system. The first one of the above equation (Eq. (5)) represents a perfectly ordered chain of identical atomic sites with energy-dependent on-site potential and hopping parameter. The second one depicts an “atomic-like” state. Each equation has its own density of states spectrum and obviously a convolution of these two will bring the true density of eigenstates of the entire system.

We have however followed an RSRG decimation scheme on the renormalized ladder (Fig. 2a). The renormalization scheme is governed by the following recursion relation:

$$\begin{aligned}\tilde{\epsilon}(n+1) &= \tilde{\epsilon}(n) + \frac{2}{\delta(n)}(f_1 + f_2), \\ \tau(n+1) &= \frac{1}{\delta(n)}(f_1 + f_2), \\ \chi(n+1) &= \frac{1}{\delta(n)}(f_3 + f_4), \\ \gamma(n+1) &= \gamma(n) + \frac{1}{\delta(n)}(f_3 + f_4).\end{aligned}\quad (6)$$

where $f_1 = [(E - \tilde{\epsilon}(n))(\tau^2(n) + \chi^2(n))]$, $f_2 = 2\tau(n)\chi(n)\gamma(n)$, $f_3 = 2(E - \tilde{\epsilon}(n))\tau(n)\chi(n)$, $f_4 = \gamma(n)(\tau^2(n) + \chi^2(n))$ and $\delta(n) = (E - \tilde{\epsilon}(n))^2 - \gamma^2(n)$. After successive steps of renormalization the potential

reaches its fixed point value. From this one can calculate the local Green function for the up and down vertices. The basic definition of the Green function [46] is as follows:

$$G = \sum_k (E - H)^{-1} |k\rangle \langle k|. \quad (7)$$

From this expression one can easily compute the local Green function as

$$G_{00}(E + i\eta) = \frac{1}{N} \sum_k \frac{1}{(E + i\eta - \epsilon^*(k))}, \quad (8)$$

where * mark denotes the fixed point value of the parameter and η is a small quantity added for the numerical calculation of DOS. From that Green's function calculation we just evaluate the local density of states using the following standard expression:

$$\rho(E) = - \left(\frac{1}{\pi} \right) \lim_{\eta \rightarrow 0} \text{Im} G_{00}(E + i\eta). \quad (9)$$

The variation of electronic density of states against energy of the electron is plotted in Fig. 4. It consists of two separate absolutely continuous sub-bands along with the coexistence of an *isolated* flat localized mode situated outside the bands. The nature of eigenstates can be easily confirmed if we just look out for the flow of overlap integral under successive RSRG iterations. A careful check of this flow pattern shows that for any energy belonging to those absolutely continuous regimes the hopping integral never goes to zero, rather follows an oscillating behavior for almost an indefinite number of iteration loops. This is a clear indication that all the states residing inside the continua are extended in nature. While for the pinned localized FB mode situated at the flank of the spectrum, the overlap parameter immediately converges to zero after few RSRG steps. This means that the overlap of the wave function with the nearest neighboring sites decays gradually. This brings a flavor of localization corresponding to $E = \epsilon_3 - \lambda$.

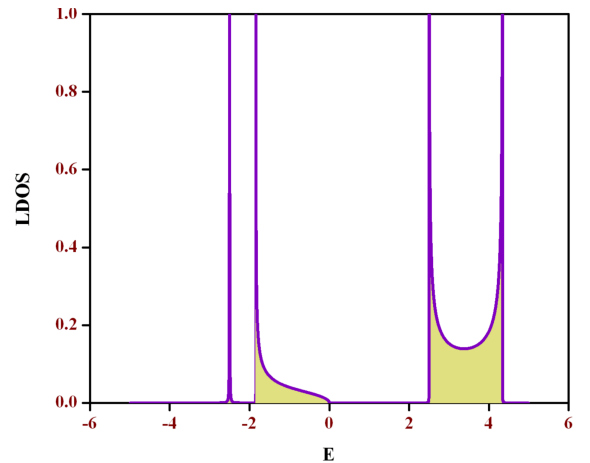


Fig. 4. Local electronic density of states profile as a function of energy. We have set the numerical values of all the on-site potentials equal to zero, i.e., $\epsilon_3 = \epsilon_4 = 0$ and $t = 1$, $\lambda = 2.5$.

2.4. Dispersion relation

Within the tight-binding framework following the RSRG method we have made it possible to confirm the non-dispersive character of that CLS. We refer to Fig. 2b. The top and the down vertices with coordination number equal to three can thus be eliminated to form an effective linear chain of identical atomic sites. Each of the atomic sites can have the on-site potential and the nearest neighbor hopping parameter of the form

$$\epsilon_0 = \epsilon_4 + \frac{4t^2(E - \epsilon_3 + \lambda)}{(E - \epsilon_3)^2 - \lambda^2},$$

$$t_0 = \frac{2t^2(E - \epsilon_3 + \lambda)}{(E - \epsilon_3)^2 - \lambda^2}. \quad (10)$$

With these effective parameters we can now easily write the tight-binding dispersion relation $E = \epsilon_0 + 2t_0 \cos ka$ which on simplification gives,

$$(E - \epsilon_3 + \lambda) \left[(E - \epsilon_4)(E - \epsilon_3 - \lambda) - 8t^2 \cos^2 \left(\frac{ka}{2} \right) \right] = 0. \quad (11)$$

From the above equation we can see the momentum independent part that gives a dispersionless FB at $E = \epsilon_3 - \lambda$. This is in accordance with the result obtained by analyzing the decoupled set of equations. The dispersion relation is plotted in Fig. 5.

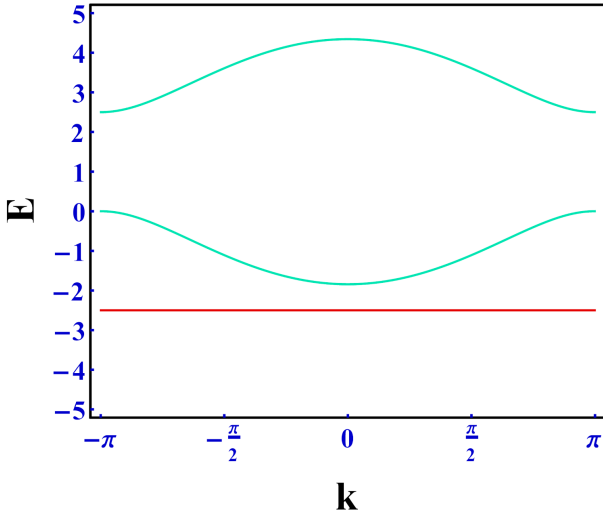


Fig. 5. The energy E vs. momentum k relation for the rhombic lattice. The non-dispersive signature of the FB state is apparent here.

From the second decoupled equation we see that there is no overlap connection with the nearest neighbouring sites and the incoming particle having such FB energy will lose its mobility. As the kinetic energy of the associated wave packet is quenched, the density of states diverges due to the relationship

$$\rho = \int v_g^{-1} d^3k. \quad (12)$$

Such divergences in the spectral profile are expected to produce anomalous behaviours in physical properties as well as transport phenomena and optical response. The singularity of spectral profile with the gradual decrease of imaginary part added to the energy for the rhombic structure is shown in the adjacent tabular form (Table I).

TABLE I

Divergence of density of states for the FB mode

| Imaginary part energy (η) | LDOS (p) |
|----------------------------------|------------|
| 10^{-2} | 15.92 |
| 10^{-3} | 159.15 |
| 10^{-4} | 1591.55 |
| 10^{-5} | 15915.49 |
| 10^{-6} | 159157.99 |
| 10^{-7} | 1588266.91 |

2.5. Transmission characteristics

For the sake of completeness of the above discussion we have also computed the two-terminal transport characteristics of the network under study (Fig. 6). The formalism is quite standard and is often used to evaluate the transport profile of several quasi-one-dimensional networks. The fundamental concept is that we have to clamp our system of finite size in between a pair of semi-infinite periodic leads, the so-called “source” and the “drain” with the corresponding lead parameters ϵ_0 and t_0 . The finite sized network sandwiched in between these two ordered leads is then successively renormalized to reduce it to an effective diatomic molecule (dimer). The two renormalized atomic sites of the dimer molecule will then have energy dependent on-site potentials and overlap parameters containing the information of the system concerned. The transmission coefficient of the lead-network-lead system then is given by a well-known formula [47]:

$$T = \frac{4 \sin^2 ka}{|\mathcal{A}|^2 + |\mathcal{B}|^2},$$

$$\text{with, } \mathcal{A} = [(M_{12} - M_{21}) + (M_{11} - M_{22}) \cos ka]$$

$$\text{and } \mathcal{B} = [(M_{11} + M_{22}) \sin ka], \quad (13)$$

where M_{ij} refer to the dimer-matrix elements, written appropriately in terms of the on-site potentials of the final renormalized left (L) and right (R) atoms at the extremities of the finite sized network and the renormalized hopping between them. $\cos ka = \frac{(E - \epsilon_0)}{2t_0}$ and a is the lattice constant in the leads which is set equal to unity throughout the calculations.

For the selective regimes of energy the transparent character of the system is justified by the high transmitting behaviour corresponding to those regions. The extended nature of the eigenstates and the consequent

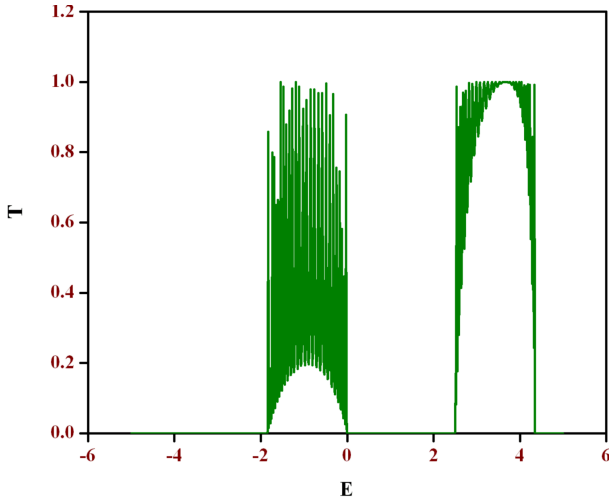


Fig. 6. Two-terminal transport characteristics against energy of the electron. We have taken the numerical values of all the on-site potentials equal to zero, i.e., $\epsilon_3 = \epsilon_4 = 0$ and $t = 1$, $\lambda = 2.5$.

chaotic oscillation of the flow of hopping integral is the reason of getting high conduction. Another fact is that the transmission shows considerably low value corresponding to the flat band energy as stated above which is expected.

3. Description of model and analysis: dimer-plaquette chain

The second example of such network we have taken is the dimer-plaquette chain as shown in Fig. 7. The network is well studied in respect of frustrated quantum Heisenberg antiferromagnetic system [48] under the influence of a high magnetic field. With a suitable Hamiltonian describing the above network they have shown the existence of dispersionless localized-magnon band. The state is localized within a characteristic *trapping cell* by virtue of phase cancellation. Inspired by this pioneering work we have taken this geometry to work out the same analytical scheme to discern the flat electronic band state following the real space renormalization group method.

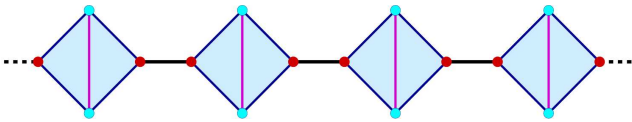


Fig. 7. An infinite array of quasi-one dimensional dimer-plaquette chain. All the sites have the same on-site parameter ϵ and inter-arm hopping is t and the vertical connection is set as λ .

In this network there exists only one type of atomic site having number of nearest neighbor equal to three. So without any loss of generality, we take the on-site

potential of all those sites as ϵ . The hopping integral along the arm of the diamond plaquette and along the dimer are taken as uniform and assigned as t , but the connection between the top and down vertices of each elementary diamond plaquette is considered as different than the others and is taken as λ .

3.1. Analytical construction of CLS

Following the same technique one can easily cast the above network into an *effective* two-arm ladder geometry with the corresponding renormalized parameters. In this case to get the effective ladder, one has to *eliminate* the two atomic sites of the dimers of the network. By virtue of this decimation process, the potential matrix now becomes

$$\epsilon = \begin{pmatrix} \epsilon + \frac{2t^2(E-\epsilon)}{\Delta} & \lambda + \frac{2t^2(E-\epsilon)}{\Delta} \\ \lambda + \frac{2t^2(E-\epsilon)}{\Delta} & \epsilon + \frac{2t^2(E-\epsilon)}{\Delta} \end{pmatrix}. \quad (14)$$

Also the hopping matrix reads as

$$t = \frac{t^3}{\Delta} \begin{pmatrix} 1 & 1 \\ 1 & 1 \end{pmatrix}, \quad (15)$$

where $\Delta = (E - \epsilon)^2 - t^2$. Here also, the potential matrix and the hopping matrix commute with each other. So following the same method, one can now decouple the composite form of the difference equation for the ladder. We will then get two linearly independent equations (in the changed basis) which are as follows:

$$\begin{aligned} \left[E - \left(\epsilon + \lambda + \frac{4t^2(E-\epsilon)}{\Delta} \right) \right] \phi_{n,1} &= \\ \frac{4t^3}{\Delta} (\phi_{n+1,1} + \phi_{n-1,1}), \\ [E - (\epsilon_3 - \lambda)] \phi_{n,2} &= 0. \end{aligned} \quad (16)$$

3.2. Density of states and transport

The first one corresponds to an effective linear chain of identical atomic sites with the renormalized on-site potential and hopping integral. The spectrum for this chain will extend from $\epsilon + \lambda + \frac{4t^2(E-\epsilon)}{\Delta} - \frac{8t^3}{\Delta}$ to $\epsilon + \lambda + \frac{4t^2(E-\epsilon)}{\Delta} + \frac{8t^3}{\Delta}$ and the bands will be populated by extended kind of eigenfunctions. (Fig. 8) This resonant character of the bands can be easily confirmed if we just check the flow of overlap parameter for any energy belonging to the *absolutely continuous* regime. It is seen that the flow of hopping never converges to zero for an indefinite number RSRG steps which is clear indicative signature of the states being extended. The other equation again represents an *atomic-like* pinned localized state for which the characteristic trapping cell is the top-down atomic dimer. The amplitudes are confined in the top and down vertices. Due to the zero amplitudes at the red colored vertices, the particle having such specific FB energy will be confined within the finite size cluster. This brings the flavor of the same CLS.

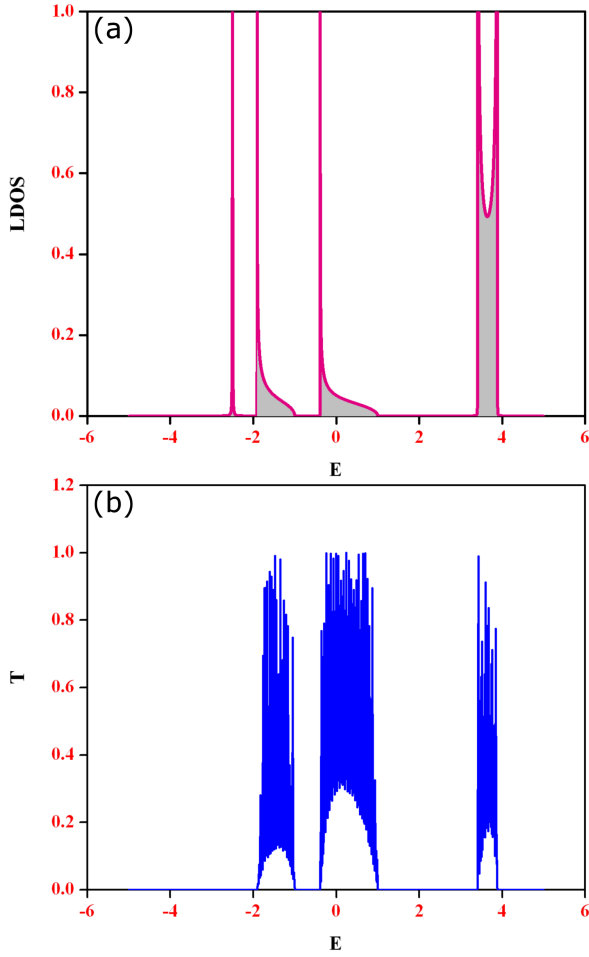


Fig. 8. (a) Local spectral landscape of dimer-plaquette chain as a function of energy. We have set the numerical values of all the on-site potentials equal to zero, i.e., $\epsilon_3 = \epsilon_4 = 0$ and $t = 1$, $\lambda = 2.5$ and (b) transmission profile against energy for the same network under the same parametric condition.

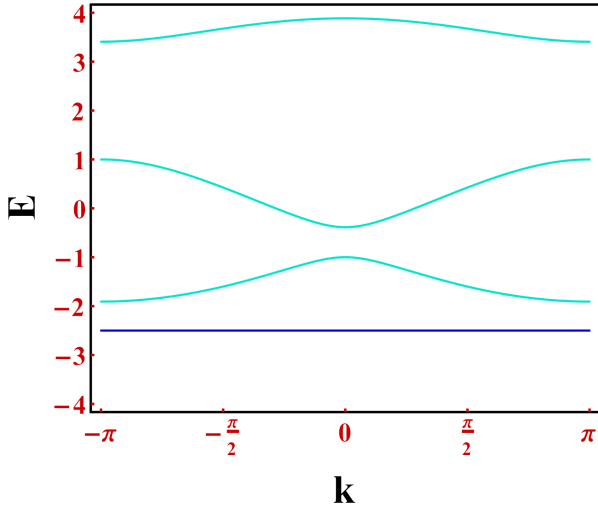


Fig. 9. Dispersion relation of dimer-plaquette chain.

3.3. Dispersion relation

To justify the non-dispersive character of this FB state constructed analytically, we will convert the structure into an effective linear chain. For this we just have to eliminate out the top and down vertices in terms of the amplitudes of the surviving sites. The tight-binding chain constructed in the above process has the renormalized parameters as follows:

$$\epsilon_0 = \tilde{\epsilon} + \frac{(\tilde{t}^2 + t^2)}{(E - \tilde{\epsilon})}, \quad t_0 = \frac{t\tilde{t}}{(E - \tilde{\epsilon})}, \quad (17)$$

where $\tilde{\epsilon} = \epsilon + \frac{2[(E-\epsilon)t^2+t^2\lambda]}{(E-\epsilon)^2-\lambda^2}$ and $\tilde{t} = \frac{2[(E-\epsilon)t^2+t^2\lambda]}{(E-\epsilon)^2-\lambda^2}$. Using the above parameters one can have the form of the dispersion relation in terms of the parameters of the original lattice as given by

$$(E - \epsilon + \lambda) [(E - \epsilon) ((E - \epsilon)(E - \epsilon - \lambda) - 4t^2) - t^2(E - \epsilon - \lambda) - 4t^3 \cos ka] = 0. \quad (18)$$

From the above expression we can see that the network supports a dispersionless flat band mode at $E = \epsilon - \lambda$ (Fig. 9).

4. Possible scope for experiment

In this section, it is very pertinent to highlight some scopes for possible experimental realization of flat photonic band in such quasi-one-dimensional structures. The recent experiments by Mukherjee et al. [28, 49] and also by the other authors [29, 50, 51] regarding the photonic analogue of localization of wave train in photonic lattices formed by laser-induced single-mode wave guides prompt us to study the method of extracting the *self-localized* modes for different model networks. The present analysis discussed in this article can be experimentally verified in this era of pretty advanced nanotechnology and lithography techniques. The wave propagation in such single-mode optical wave guides can be adjusted by femtosecond laser-writing method as well as the optical induction technique. The overlap parameter can be manipulated by the dielectric properties of the core material. This provides a scope for direct observation of diffraction free FB states. Also, a synthetic gauge field [52, 53] can be generated by modulating the propagation constant to study the effect of magnetic field in our proposed geometry.

4.1. Photonic analogue

Analogy between the electronic model and the corresponding photonic scenario within the tight-binding framework is not new. As first introduced by Sheng et al. [54, 55], the wave propagation through any quasi-one-dimensional network can be exactly mapped back onto the corresponding electronic case with the appropriate parametric substitution. The analogy [31, 56] of the network equations with that of an electron propagating in a similar lattice helps us to study the localization of classical waves. Also, this mapping is entirely a mathematical

construction and once this is done the RSRG recursion relations are insensitive to whether the input comes from a quantum case or a classical one. Obviously here the propagation of classical wave can be manipulated by selective choice of dielectric parameter. If we set the length of the wave guide segment at the very outset, then one can easily compute the *exact* frequency of injected wave train for which the self-localization occurs.

4.2. Optical density of modes

We have cited the distribution of allowed photonic modes using the tight-binding analogy. The profile showing the local density of photonic modes (LDPM) is plotted as a function of frequency of the injected signal within the range $0 < \omega/2\pi c < 1/2$. The plot shows clusters of nonzero values of LDPM over different subband regimes. It is needless to say that quite arbitrarily we have taken the index of refraction of the core of the wave guide as $n = \sqrt{3}$. Both the networks also exhibit gaps in between two subbands and thus can be a suitable candidate for photonic bandgap kind of system. Figure 10a and Fig. 11a show the density of optical modes for rhombic lattice and dimer-plaquette chain, respectively.

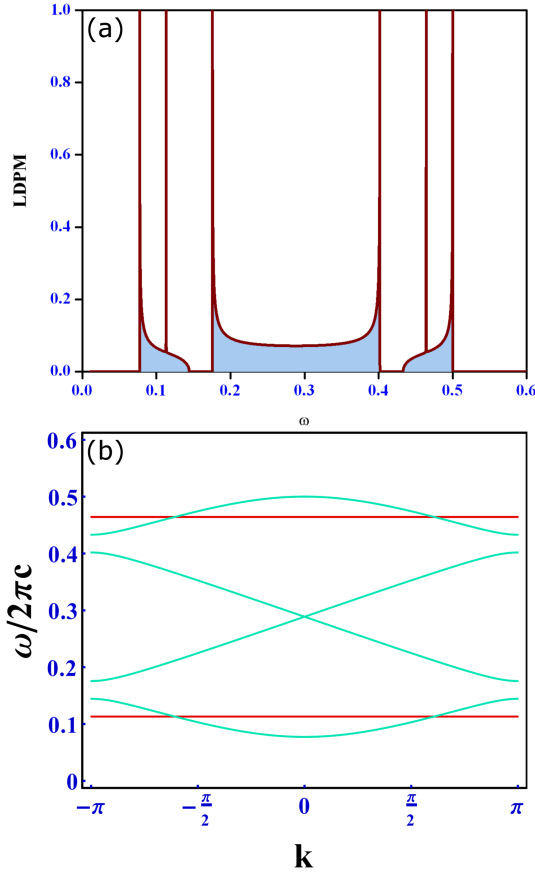


Fig. 10. (a) Local density of photonic modes as a function of the frequency of the wave injected for the wave guide network arranged in AB_2 rhombic geometry and (b) the corresponding optical dispersion relationship.

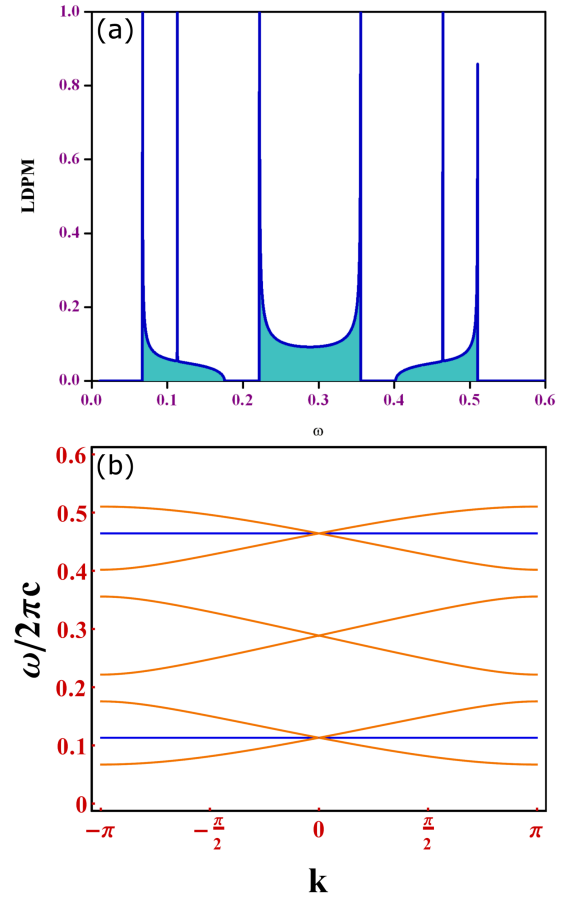


Fig. 11. (a) Local density of photonic modes against the frequency of the signal for the wave guide network arranged in dimer-plaquette chain geometry and (b) the corresponding photonic dispersion relationship.

4.3. Flat photonic modes

Because of zero group velocity, the corresponding single-particle state is sharply localized at a point, or in a finite cluster of nodal points in the system. Such clusters are separated from the neighboring clusters by vertices where the amplitude of the wave function is zero. Therefore, the movement of the particle is restricted along the periphery of those finite clusters.

By virtue of the decoupled equations and optical analogue of the tight-binding dispersion relation one can easily compute the flat photonic modes for the monomode wave guide network using the one-to-one correspondence of electronic and photonic cases. For $\epsilon_r = 3$, the non-dispersive roots are $\omega/2\pi c = 0.113, 0.465$. Those two roots correspond to the left and right spikes appearing in the DOS spectrum.

In photonics flat bands are closely related to the technologically-important concept of slow light, where the significant decrease in the wave group velocity offers enhanced nonlinear effects and is useful for pulse buffering. If a single optical mode is non-dispersive in one direction, it implies localization in that direction as an extreme case, unfolding the possibility of engineering

ultraslow light. This is the ultimate consequence of a perfect geometric phase cancellation which causes effective mass tensor to be divergent, leading to a possible observation of “heavy photons”. This does not appear improbable if we borrow the language for the electrons, thanks to the analogous tight-binding model which indeed works quite accurately for the low-lying photonic dispersion. Vanishing curvature in the frequency (ω) vs. wave vector (k) curves signifies infinite effective mass of the particle involved. This in turn makes the mobility vanish. Due to the vanishing group velocity of the *heavy photon* the curvature of the band corresponding to those modes becomes completely flat in nature.

4.4. Slow light and mode crossover

Light plays a very important as well as effective role as a messenger in the communication system and optical communication is one of the well-studied aspect in the technological field. Slow light with a remarkably low group velocity of the wave train is a very promising solution for optical delay line or optical buffering and advanced time-domain optical signal processing. It is also anticipated to enhance linear and nonlinear effects [58] and so miniaturize functional photonic devices, as slow light compresses optical energy in space that eventually increases the light-matter interaction. This in turn, results in enhanced gain and absorption, phase shift, and non-linearities. The flat band networks as discussed in the previous section support one or more dispersionless bound states. For those specific states the particle is locked in space. This observation gives oxygen to the photonic flat band researchers who try to achieve a slow light condition by enforcing destructive interference. By virtue of this phase cancellation induced by topological symmetry present in the underlying structure, the velocity of the light can be slowed down considerably [30]. This amounts to a photonic realization of the flat-band model in solid-state physics as conceived by Lieb [3], Mielke [59], and Tasaki [6].

The vanishing curvature of the flat band indicates extremely low group velocity. The dense packing of the flat and the dispersive bands therefore opens up a possibility of slow light engineering and re-entrant intermodal crossover of optical eigenmodes, going from a resonant or diffusive (dispersive) state to a sharply localized or bound (flat) one, or vice versa as one climbs the frequency axis at any fixed value of the wave vector k . Such a crossover can, in principle, be manipulated over arbitrarily small intervals of frequency. The entire network can thus behave like an optical switch which selectively goes off (for a localized, non-dispersive bound state) and on (for a resonant state) over arbitrary small frequency intervals.

5. Concluding remarks

We have shown an analytically exact scheme to extract the eigenvalues corresponding to the compact localized, non-dispersive, degenerate flat band eigenstates of a set

of quasi-one-dimensional structures. A real space renormalization group scheme is exploited to unravel such dispersionless sharply localized states. The evaluation of spectral landscape is corroborated by the numerical calculation of two-terminal transport. The flat curvature of energy band corresponding to those *self-localized* is demonstrated using the exact computation of dispersion profile within the same tight-binding formalism.

One-to-one mapping of electronic scenario onto the corresponding optical case prompts us to identify the analogous photonic flat band modes for the same geometry arranged in a single-mode optical waveguide structure. Such results bring an opportunity to modulate experimentally the localization of classical waves, for example, light, triggered by the lattice topology without bothering about the high permittivity of the core materials. It might be useful in developing novel photonic band-gap structures. Also, the physical significance of vanishing group velocity is that several scattering waves form standing wave pattern in such photonic wave guide network. For such self-localized eigenmodes, we can obtain coherent waves, i.e., lasing action [60, 61] at the photonic band edges.

Acknowledgments

A.N. is thankful for the stimulating discussions regarding the results with Prof. Arunava Chakrabarti.

References

- [1] P.W. Anderson, *Phys. Rev.* **109**, 1492 (1958).
- [2] B. Sutherland, *Phys. Rev. B* **34**, 5208 (1986).
- [3] E.H. Lieb, *Phys. Rev. Lett.* **62**, 1201 (1989).
- [4] A. Mielke, *J. Phys. A* **24**, L73 (1991).
- [5] A. Mielke, *J. Phys. A* **24**, 3311 (1991).
- [6] H. Tasaki, *Phys. Rev. Lett.* **69**, 1608 (1992).
- [7] A. Mielke, H. Tasaki, *Commun. Math. Phys.* **158**, 341 (1993).
- [8] H. Tasaki, *Prog. Theor. Phys.* **99**, 489 (1998).
- [9] E. Kapit, E. Mueller, *Phys. Rev. Lett.* **105**, 215303 (2010).
- [10] E. Tang, J.W. Mei, X.G. Wen, *Phys. Rev. Lett.* **106**, 236802 (2011).
- [11] K. Sun, Z. Gu, H. Katsura, S. Das Sarma, *Phys. Rev. Lett.* **106**, 236803 (2011).
- [12] T. Neupert, L. Santos, C. Chamon, C. Mudry, *Phys. Rev. Lett.* **106**, 236804 (2011).
- [13] W. Yao, S.A. Yang, Q. Niu, *Phys. Rev. Lett.* **102**, 096801 (2009).
- [14] I. Bloch, J. Dalibard, W. Zwerger, *Rev. Mod. Phys.* **80**, 885 (2008).
- [15] D.N. Christodoulides, F. Lederer, Y. Silberberg, *Nature* **424**, 817 (2003).
- [16] N. Masumoto, N.Y. Kim, T. Byrnes, K. Kusudo, A. Löffler, S. Höfling, A. Forchel, Y. Yamamoto, *New J. Phys.* **14**, 065002 (2012).

- [17] R.G. Dias, J.D. Gouveia, *Sci. Rep.* **5**, 16852 (2015).
- [18] L. Morales-Inostroza, R.A. Vicencio, *Phys. Rev. A* **94**, 043831 (2016).
- [19] A. Ramachandran, A. Andreanov, S. Flach, *Phys. Rev. B* **96**, 161104 (2017).
- [20] C. Xu, G. Wang, Z.H. Hang, J. Luo, C.T. Chan, Y. Lai, *Sci. Rep.* **5**, 18181 (2015).
- [21] S. Flach, D. Leykam, J.D. Bodyfelt, P. Matthies, A.S. Desyatnikov, *Europhys. Lett.* **105**, 30001 (2014).
- [22] W. Maimaiti, A. Andreanov, H.C. Park, O. Gendelman, S. Flach, *Phys. Rev. B* **95**, 115135 (2017).
- [23] S.Q. Shen, Z.M. Qiu, G.S. Tian, *Phys. Rev. Lett.* **72**, 1280 (1994).
- [24] C. Wu, D. Bergman, L. Balents, S.D. Sarma, *Phys. Rev. Lett.* **99**, 070401 (2007).
- [25] S. Miyahara, S. Kusuta, N. Furukawa, *Physica C* **460**, 1145 (2007).
- [26] A. Julku, S. Peotta, T.I. Vanhala, D.H. Kim, P. Törmä, *Phys. Rev. Lett.* **117**, 045303 (2016).
- [27] N.B. Kopnin, T.T. Heikkilä, G.E. Volovik, *Phys. Rev. B* **83**, 220503 (2011).
- [28] S. Mukherjee, A. Spracklen, D. Choudhury, N. Goldman, P. Öhberg, E. Andersson, R.R. Thomson, *Phys. Rev. Lett.* **114**, 245504 (2015).
- [29] R.A. Vicencio, C. Cantillano, L. Morales-Inostroza, B. Real, C. Mejía-Cortés, S. Weimann, A. Szameit, M.I. Molina, *Phys. Rev. Lett.* **114**, 245503 (2015).
- [30] S. Endo, T. Oka, H. Aoki, *Phys. Rev. B* **81**, 113104 (2010).
- [31] A. Nandy, A. Chakrabarti, *Phys. Rev. A* **93**, 013807 (2016).
- [32] M. Goda, S. Nishino, H. Matsuda, *Phys. Rev. Lett.* **96**, 126401 (2006).
- [33] A. Mielke, *J. Phys. A Math. Gen.* **25**, 4335 (1992).
- [34] A. Nandy, B. Pal, A. Chakrabarti, *J. Phys. Condens. Matter* **27**, 125501 (2015).
- [35] R.A. Vicencio, C. Mejía-Cortés, *J. Opt.* **16**, 015706 (2014).
- [36] S. Rojas-Rojas, L. Morales-Inostroza, R.A. Vicencio, A. Delgado, *Phys. Rev. A* **96**, 043803 (2017).
- [37] S. Xia, Y. Hu, D. Song, Y. Zong, L. Tang, Z. Chen, *Opt. Lett.* **41**, 1435 (2016).
- [38] J.V. Neuman, E. Wigner, *Phys. Z.* **30**, 467 (1929).
- [39] F.H. Stillinger, D.R. Herrick, *Phys. Rev. A* **11**, 446 (1975).
- [40] Y.E. Kraus, Y. Lahini, Z. Ringel, M. Verbin, O. Zilberberg, *Phys. Rev. Lett.* **109**, 106402 (2012).
- [41] Y. Lahini, R. Pugatch, F. Pozzi, M. Sorel, R. Morandotti, N. Davidson, Y. Silberberg, *Phys. Rev. Lett.* **103**, 013901 (2009).
- [42] M. Ochi, R. Arita, M. Matsumoto, H. Kino, T. Miyake, *Phys. Rev. B* **91**, 165137 (2015).
- [43] I. Hase, T. Yanagisawa, K. Kawashima, *Nanoscale Res. Lett.* **13**, 63 (2018).
- [44] J.D. Bodyfelt, D. Leykam, C. Danieli, X. Yu, S. Flach, *Phys. Rev. Lett.* **113**, 236403 (2014).
- [45] M. Hyrkäs, V. Apaja, M. Manninen, *Phys. Rev. A* **87**, 023614 (2013).
- [46] S. Souma, A. Suzuki, *Phys. Rev. B* **65**, 115307 (2002).
- [47] Y. Liu, K.A. Chao, *Phys. Rev. B* **34**, 5247 (1986).
- [48] O. Derzhko, J. Richter, O. Krupnitska, T. Krokhamalskii, *Phys. Rev. B* **88**, 094426 (2013).
- [49] S. Mukherjee, R.R. Thomson, *Opt. Lett.* **40**, 5443 (2015).
- [50] S. Xia, Y. Hu, D. Song, Y. Zong, L. Tang, Z. Chen, *Opt. Lett.* **41**, 1435 (2016).
- [51] Y. Zong, S. Xia, L. Tang, D. Song, Y. Hu, Y. Pei, J. Su, Y. Li, Z. Chen, *Opt. Expr.* **24**, 8877 (2016).
- [52] S. Longhi, *Opt. Lett.* **39**, 5892 (2014).
- [53] S. Longhi, *Opt. Lett.* **38**, 3570 (2013).
- [54] S. Alexander, *Phys. Rev. B* **27**, 1541 (1983).
- [55] Z.Q. Zhang, P. Sheng, *Phys. Rev. B* **49**, 83 (1994).
- [56] B. Pal, P. Patra, J.P. Saha, A. Chakrabarti, *Phys. Rev. A* **87**, 023814 (2013).
- [57] D. Leykam, A. Andreanov, S. Flach, *Adv. Phys. X* **3**, 1473052 (2018).
- [58] T. Baba, *Nat. Photon.* **2**, 465 (2008).
- [59] A. Mielke, *Phys. Lett. A* **174**, 443 (1993).
- [60] M. Imada, S. Noda, A. Chutinan, T. Tokuda, M. Murata, G. Sasaki, *Appl. Phys. Lett.* **75**, 316 (1999).
- [61] M. Meier, A. Mekis, A. Dodabalapur, A. Timko, R.E. Slusher, J.D. Joannopoulos, O. Nalamasu, *Appl. Phys. Lett.* **74**, 7 (1999).